Geotechnical and Geological Engineering
An International Journal

Editors

Editors-in-Chief:

James L. Hanson
California Polytechnic State University, San Luis Obispo, CA, USA email: jahanson@calpoly.edu

Pinnaduwa H. S. W. Kulatilake
Jiangxi University of Science and Technology, Ganzhou, China & The University of Arizona, Tucson, AZ, USA email: kulatila@u.arizona.edu

Interim Editor-in-Chief:

David Toll
Durham University, UK; email: d.g.toll@durham.ac.uk

Associate Editors:

N. Consoli, Federal University of Rio Grande do Sul, Porto Alegre, Brazil; **M. Diederichs**, Queen's University, Kingston, Canada; **T. Katsumi**, Kyoto University, Japan; **K. Sobhan**, Florida Atlantic University, Boca Raton, FL, USA

Editorial Board:

M. Berilgen, Yildiz Technical University, Istanbul, Turkey; **M. Bouassida**, National Engineering School of Tunis, Tunisia; **G. Cai**, Southeast University, China; **D. Choudhury**, Indian Institute of Technology Bombay, India; **G.B. Crosta**, University of Milan, Italy; **D. Debasis**, Indian Institute of Technology Kharagpur, India; **J. Delgado Rodrigues**, National Laboratory of Civil Engineering, Lisbon, Portugal; **A. Gens**, Polytechnic University of Catalonia, Barcelona, Spain; **S. Grasso**, University of Catania, Italy; **L. Li**, Tennessee State University, Nashville, TN, USA; **M. Manassero**, Polytechnic University of Turin, Italy; **V. Marinos**, National Technical University of Athens, Greece; **M.R. Massimino**, University of Catania, Italy; **L. Di Matteo**, University of Perugia, Italy; **E.C. Shin**, Incheon National University, Republic of Korea; **G. Spagnoli**, DMT

Instructors

Librarians (Springer Nature)

Societies and Publishing Partners

Advertisers

Shop on Springer.com

About Springer

About us

Help & Support

Contact us

Press releases

Impressum

Legal

General term & conditions

California Privacy Statement

Rights & permissions

Privacy

How we use cookies

Manage cookies/Do not sell my data

Accessibility

Not logged in - 103.3.46.176
Universitas Lampung (3991463632)

SPRINGER NATURE

© 2022 Springer Nature Switzerland AG. Part of Springer Nature.

Geotechnical and Geological Engineering
An International Journal

Aims and scope

Geotechnical and Geological Engineering publishes papers in the areas of soil and rock engineering and also of geology as applied in the civil engineering, mining and petroleum industries. The emphasis is on the engineering aspects of soil and rock mechanics, geology and hydrogeology, although papers on theoretical and experimental advances in ground mechanics are also welcomed for inclusion.

The journal encompasses a broad spectrum of geo-engineering although several areas have been identified which will be given particular priority:

Soil and rock engineering;

Foundation engineering;

Applied geology for design and construction;

Geo-environmental engineering;

Earthquake engineering and dynamic behavior of soils and rocks;

Geohazards and mitigation;

Mining engineering;

Geotechnical aspects of petroleum engineering;

Information technology applications in geo-engineering;

Novel geotechnical construction techniques;

Case histories describing important geo-engineering projects.

Geotechnical and Geological Engineering publishes contributions in the form of original and review papers,

Springer Link

Search Log in

Geotechnical and Geological Engineering

An International Journal

Volume 39, issue 8, December 2021

38 articles in this issue

Obituary of Professor Paul (Pavlos) Marinos

David G. Toll

Obituary | Published: 03 November 2021 | Pages: 5427 - 5428

A Review on Chemical Stabilization of Peat

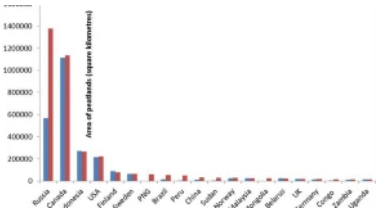

Suhail Ahmad Khanday, Monowar Hussain & Amit Kumar Das

State-of-the-Art Review | Published: 22 May 2021 | Pages: 5429 - 5443

On the Application of the Novel Thin Spray-on Liner (TSL): A Progress Report in Mining Operations

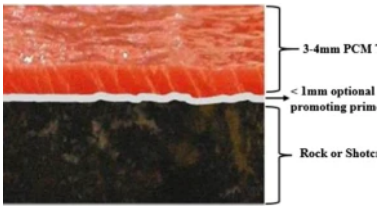

Peter Kolapo, Moshood Onifade ... Praise Oluwatomisin Akinseye

State-of-the-Art Review | Published: 30 May 2021 | Pages: 5445 - 5477

Dynamic Response and Mechanical Behaviours of Geogrid for High Earth-rockfill Dams

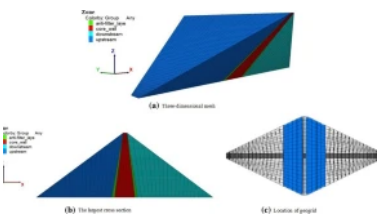

Yalin Zhu, Chi Ma ... Yixian Wang

Original Paper | Published: 12 June 2021 | Pages: 5479 - 5492

Investigation on the Surface Settlement of Curved Shield

Soil

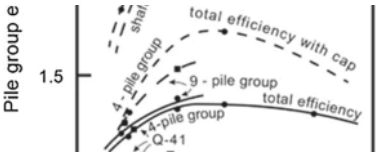

Wilson Cartaxo Soares, Roberto Quental Coutinho & Renato Pinto da Cunha

Original Paper | Published: 21 May 2021 | Pages: 5599 - 5618

Influence of Acid Attack on Physical Characteristics of Cemented Tailings Backfill

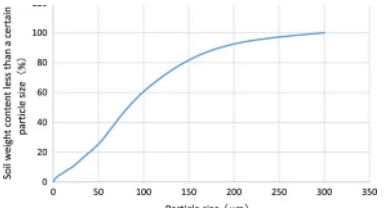

Yong-gang Huang, Gui-yao Wang ... Wei-peng Liu

Original Paper | Published: 17 May 2021 | Pages: 5619 - 5631

Wetting Induced Deformation of Soils Triggering Landslides in Pakistan

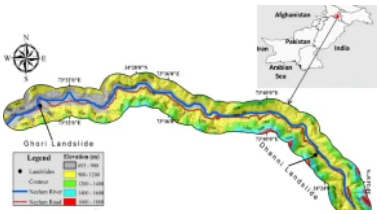

Saima Riaz, Mamoru Kikumoto ... Andius Dasa Putra

Original Paper | Published: 10 July 2021 | Pages: 5633 - 5649

Reliability Assessment of Shallow Foundation Stability Under Eccentric Load Using Monte Carlo and First Order Second Moment Method

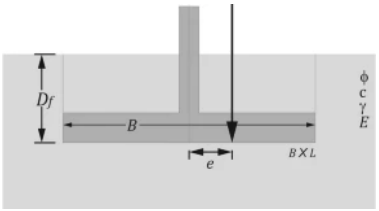

Sina Fatolahzadeh & Rasool Mehdizadeh

Original Paper | Published: 20 May 2021 | Pages: 5651 - 5664

Experimental Study on the Sand of Bandar-e Anzali Using Shaking Table

Farzad Farrokhzad, Ebrahim Golpour ... Asskar Janalizadeh Choobbasti

Original Paper | Published: 25 May 2021 | Pages: 5665 - 5674

Landslide Susceptibility Mapping Using GIS-based Fuzzy Logic and the Analytical Hierarchical Processes Approach: A Case Study in Constantine (North-East Algeria)

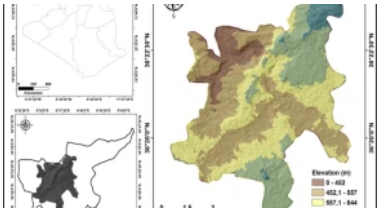

Amina Abdı, Ali Bouamrane ... Anouar Kaouachi

Original Paper | Published: 28 July 2021 | Pages: 5675 - 5691

Study on Crack Evolution Laws of Rock-Like Material with Double Cracks Under Semi-circular Bending

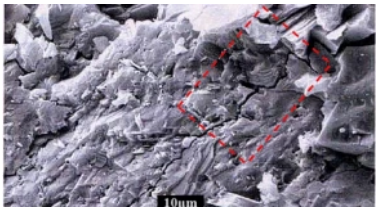

Zhitao Zhang & Enbin Yang

Original Paper | Published: 23 May 2021 | Pages: 5693 - 5705

Effects of Portal Failure on Tunnel Support Systems in a Highway

Geotech Geol Eng
https://doi.org/10.1007/s10706-021-01851-7

ORIGINAL PAPER

Wetting Induced Deformation of Soils Triggering Landslides in Pakistan

Saima Riaz · Mamoru Kikumoto · Muhammad Basharat · Andius Dasa Putra

Received: 10 May 2019 / Accepted: 12 May 2021
© The Author(s), under exclusive licence to Springer Nature Switzerland AG 2021

Abstract Shallow and deep seated landslides in natural slopes are often induced by rainfall. The cause of the failure is usually considered to be due to the decrease in effective confining stress due to a suction loss by water infiltration. However, rainwater infiltrates into the slope surface resulting in a reduction of shear strength of soil and deformation and failure may occur even without significant change in effective stress. It is thus essential to examine the deformation and failure characteristics of the soil induced by wetting. This study investigates on the wetting-induced deformations under isotropic compression condition and triaxial shearing condition using a triaxial test apparatus for unsaturated soils. Two soil samples collected from the active landslide sites from Pakistan were used to examine both the shear strength and deformation behavior during water infiltration at different levels of deviatoric stress by keeping the deviatoric stress constant during the water infiltration stage. The test results showed that, even though the deviatoric stress is kept constant during water permeation at different stress levels, the distortional deformation was exhibited due to wetting by a significant amount for both samples. The effect of water infiltration on the deformation behavior of unsaturated soil regarding the change in the degree of saturation and void ratio was also observed. There was a decrease in the void ratio for both specimens during increasing the degree of saturation at different level of deviatoric stress ratio. Under higher deviator stress, more decrease in void ratio and an increase of the degree of saturation were observed. Therefore, it can be said that deformation of soil due to water infiltration is a critical phenomenon and it should be considered while analyzing the soil behavior due to water infiltration by rainfall or rise in groundwater level, even if the slope is not failed, significant deformations may hinder the performance of natural slopes.

Keywords Landslide · Rainfall · Wetting-induced deformation · Deviator stress · Triaxial test

S. Riaz
University of Engineering and Technology, Lahore, Pakistan

S. Riaz · M. Kikumoto (✉) · A. D. Putra
Yokohama National University, Yokohama, Japan
e-mail: kikumoto-mamoru-fc@ynu.ac.jp

M. Basharat
University of Azad Jammu and Kashmir, Muzaffarabad, Pakistan

A. D. Putra
University of Lampung, Lampung, Indonesia

1 Introduction

Geologically and tectonically active Himalayan Range is characterized by highly elevated mountains

Published online: 10 July 2021

and deep river valleys. Because of steep mountain slopes and dynamic geological conditions, landslides are widespread in sub and Lesser Himalayas zones of Pakistan. Landslide is one of the most common hazards in the Himalayas and can be particularly devastating when it occurs adjacent to human settlements and infrastructures, such as towns, roads, bridges, and utilities. The Kashmir area is characterized by rugged terrain and therefore most of the road network, is carved out on slopes, leading to slope instability and eventually landslide (Fig. 1). The significant portion of the road network in the region is at risk, because of the landslide hazard (Fig. 2a–d).

Triggering factors such as torrential monsoon rains, and floods greatly aggravate slope instability mainly along the road network (Rahman et al. 2014; Sudmeier-Rieux et al. 2011; Aydan et al. 2009; Bulmer et al. 2007; Owen et al. 2008; Petley et al. 2006a, b; Schneider 2009; Fujiwara et al. 2006). Dahal and Hasegawa (2008) predicted a long-term slope destabilization due to the monsoonal climatic conditions and the vulnerable nature of the destabilized slopes. They stated that extensive fracturing of dolomites in Muzaffarabad indicates that, in the future, slope failures can be easily triggered by heavy rainfall or low-intensity earthquakes. Muzaffarabad will experience a significant increase in landslide area in the subsequent monsoon seasons because of the presence of extensive slope cracks (Petley et al. 2006a, b; Shafique et al. 2016).

Muzaffarabad receives heavy rain during monsoon season each year. Figure 3a) shows the monthly rainfall patterns at Muzaffarabad station and number of landslides in District Muzaffarabad AJK, Pakistan from 2004 to 2008. Precipitation data were obtained from the Pakistan metrological Department, Lahore office and landslide data were taken from the planning and development department, AJK. It is shown that the monsoon season starts from June and ends at the end of August (heavy rainfall occurs with monthly extremes of up to 620 mm). In September, rainfall declines, and by November conditions are dry, with minimal rainfall of 30 mm/month. January to May is also dry months in the region.

Figure 3b shows the data of the number of landslides per month from 2004 to 2008. The data

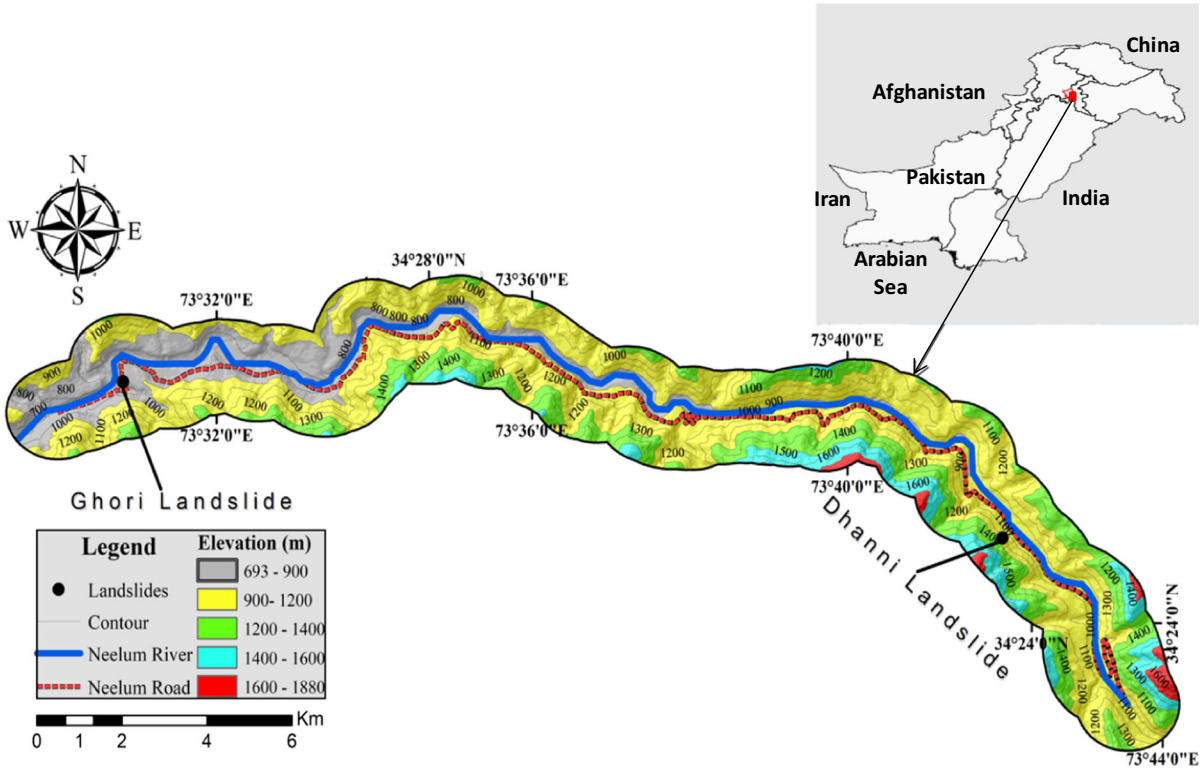

Fig. 1 Geographical location of the study area

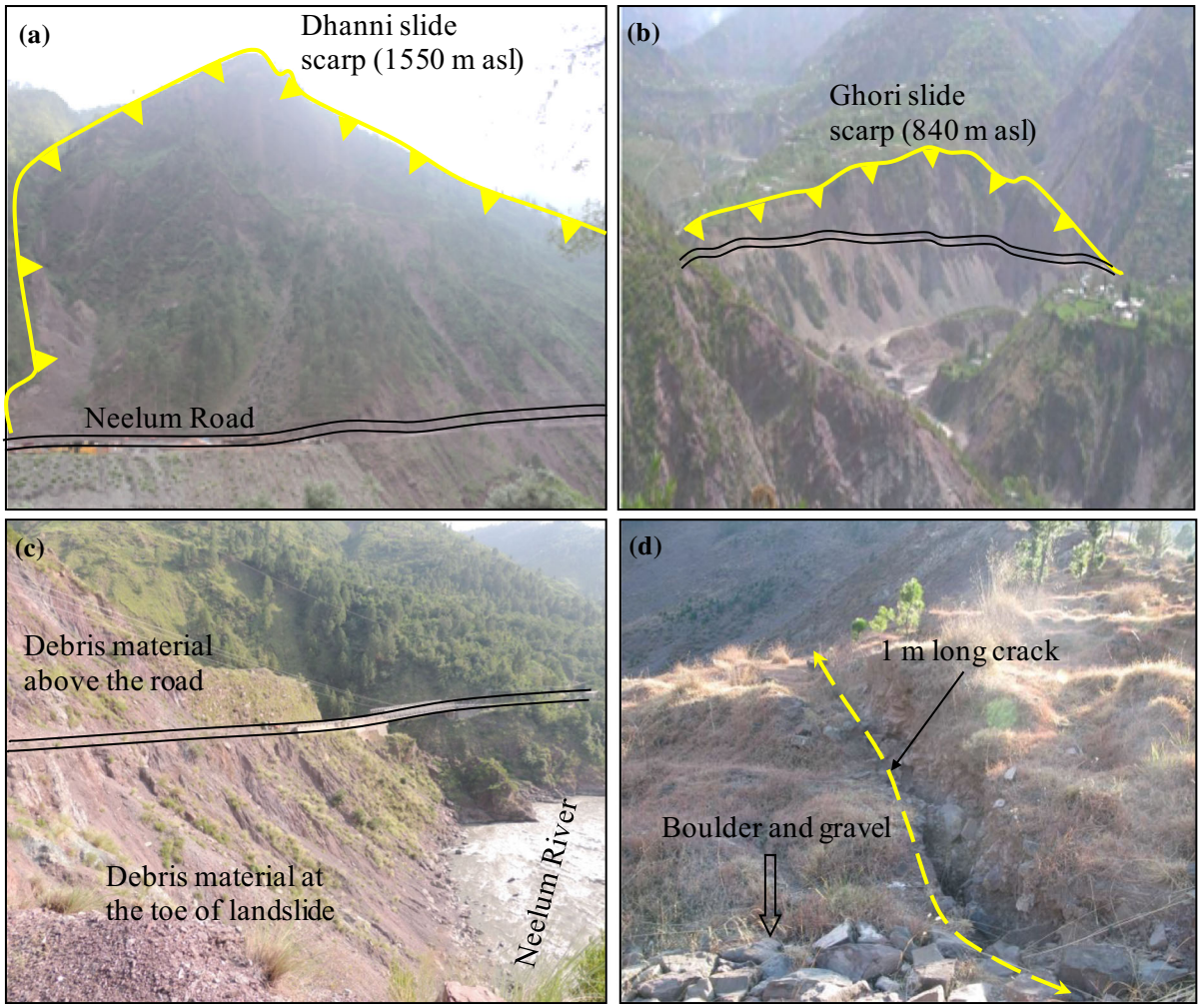

Fig. 2 **a** Overview of Dhanni landslide. **b** Overview of Ghori landslide. **c** Material deposited above the main road and toe of the Ghori landslide. **d** 1 m long crack on the scarp of Dhanni landslide

shows that even before the 2005 Kashmir earthquake, there were many landslides during the monsoon season of the year 2004. After Kashmir earthquake in October 2005, numbers of landslides were drastically increased during the monsoon seasons of years 2006, 2007, and 2008 as described by Riaz et al. (2019), Saba et al. (2010), Kamp et al. (2010), Konagai et al. (2009) and Rahman et al. (2014) in their studies.

Extensive fissuring in the valley slopes together with the freshly mobilized landslide debris constitutes a potential hazard in the coming snowmelt and monsoon seasons. Pore water pressure can easily rise in this debris and result in a massive landslide during the following monsoon seasons (Konagai and Sattar 2011; Sato et al. 2007; Schneider 2009; Owen et al. 2008). Osanai et al. (2009) conducted a statistical study on 19,035 cases of landslides between 1972 and 2007 in Japan. They reported that 93% of those landslides were caused by heavy rainfall. Therefore, the demand for early warning methods and rainfall-induced failure and post-failure mechanisms against landslides is on rising in every country. Two active landslides (Ghori and Dhanni landslides) are selected for this study because the present trends of prioritizing natural disasters in Pakistan shows the landslide occurrences along the major highways, especially the route mentioned above is given much importance. It is due to higher economic loss as well as a more significant number of people affected, especially due to traffic disruption, during an event of roadside

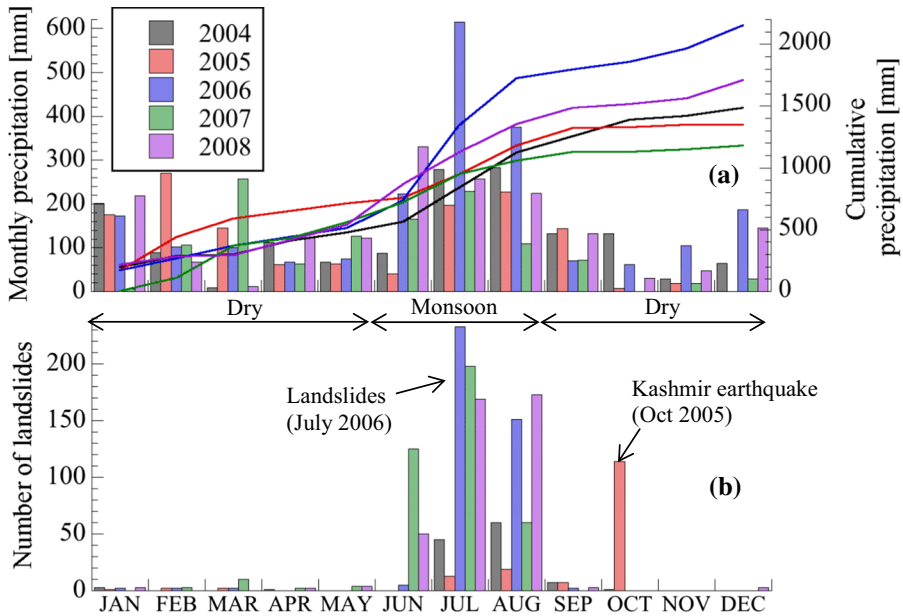

Fig. 3 **a** Rainfall characteristics at Muzaffarabad station and **b** number of landslides in District Muzaffarabad AJK, Pakistan from 2004 to 2008

failure. These landslides were trigerred during the monsoon of 2006 followed by flood in AJK on 28 July 2006 which obliterated four houses and six shops in a village close to Muzaffarabad alongwith 12 temporary shelters in the nearby village were also flattened (Planning and Development Department, AJK). The Neelum Valley Road winding through the mountainous region in northeast of Muzaffarabad is blocked for traffic for more than a week, with long patches having been wiped out by rains. These landslides were triggered during torrential rains and flood, so there was a need to explore the failure mechanism of these landslides due to wetting induced deformations. Evaluation of the wetting-induced deformation of a slope or foundation is crucial because the results are used to calculate the magnitude of the corresponding ultimate bearing capacity or to determine appropriate deformation control methods.

Wetting-induced deformation can generate deep cracks that significantly weaken the structure (Albrecht and Benson 2001; DeCarlo and Shokri 2014). Subsequently, these cracks may generate water leakage channels and threaten the safety of the structure (Zhang et al. 2016, Tang et al. 2016; Leonards and Davidson 1984). There are many factors that significantly influence the deformation induced by wetting such as soil type, ratio of wetting, initial matric suction, degree of saturation, dry unit weight, and stress condition (Miller et al. 2001; Lim and Miller 2004; Wang and Sassa 2001; Prakoso 2013; Elsharief et al. 2016; Zhang et al. 2017; Nishigata et al. 2003). There are numerous studies concerning the influence of wetting on stress–strain behavior of unsaturated soils (Jennings and Burland 1962; Kato and Ohnaka 2000; Ferber et al. 2008; AiroFarulla et al. 2010; Sun et al. 2007; Bishop and Donald 1961). The majority of these works have been executed through oedometer apparatus. However, the application of this apparatus presents certain limitations concerning, stress and strain boundary conditions. For removing the limitations as mentioned above, triaxial apparatus has been used by some authors such as Anderson and Riemer (1995), Sun et al. (2007), Meen and Young (2014) and Meilani et al. (2005). The effect of different factors affecting the wetting and deformation of soils such as stress path, density, drainage conditions can be studied by triaxial apparatus. An important issue corresponding to the majority of practical geotechnical problems is the wetting of unsaturated soils in natural slopes under a constant deviatoric stress state and wetting–induced volumetric deformation during the time. This aspect is the aim of the present work. Therefore, in this study, the effects of water infiltration on the deformation of two kinds of soils collected from actual

landslide sites were investigated at different deviatoric stress ratios under the anisotropic stress state and at same initial relative density through a series of consolidated drained (CD) triaxial tests. The results on the effect of stress ratio on the volumetric and distortional behavior due to wetting are also presented.

2 Geology of the Study Area

The study area lies in the Murree Formation (Fig. 4). The Murree Formation covering the 52% of the Kashmir region, is comprised of Miocene interbedded sandstones, siltstones, claystone and shales and host majority of the rain-induced landslides (50%—Sato et al. 2007; 63%—Kamp et al. 2008; 65%—Ray et al. 2009; 57%—Peduzzi 2010 and 67.4%—Basharat et al. 2014). The high concentration of landslides on Murree Formation can partly be also attributed to the anthropogenic activities (roads), larger spatial coverage, Torrential rains and floods during monsoon season. The area underlain by the Murree Formation is also declared and observed as the most susceptible to the future landslide (Guzzetti et al. 1999).

3 Landslide Mapping

Three field visits were carried out for detail landslide mapping and soil sample collection. The first field visit was carried out in May 2016 for reconnaissance survey and to identify the active landslides along the Neelum road from the information given by the Planning and Development Department, Azad Jammu and Kashmir (AJK). Field mapping included scarp and body of the landslide. During the field visit, it was observed that Ghori and Dhanni landslides are the large-scale landslides that caused the road blockage for the continuity of the traffic along this road every monsoon season. The second field visit was carried out in September 2016 to document the landslides in detail. Moreover, the construction of longitudinal and cross profiles was performed. The third field visit was carried out in March 2017 for collecting soil samples for laboratory testing. Global Positioning System (GPS), Laser Distance Meter, clinometer, Brunton compass, and tape measurement were used during field investigation. Landslide photographs have been taken to document the landslide features.

Ghori and Dhanni landslides have been mapped on scale 1:1500 and 1:5000 respectively as shown in Fig. 5a, b. The distinct lithological units have been identified and mapped. The lithological units and geological formations have also been presented on the maps with bedding attitude where available. Brunton compass was used to measure the attitude of beds. The landslide segments have been demarcated by taking GPS points in the field. The length and width of landslides was measured using Laser distance meter (Reigl-F-21 H) with accuracy of 15 cm. The slope angle was measured by using clinometer. The field observations regarding landslides were also noted, during the field survey.

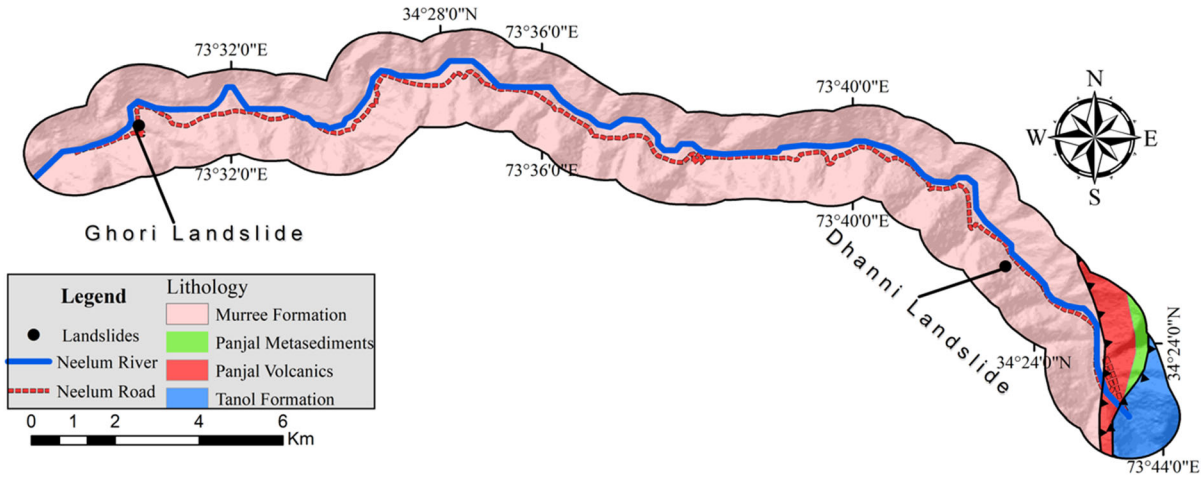

Fig. 4 Geology of the study area

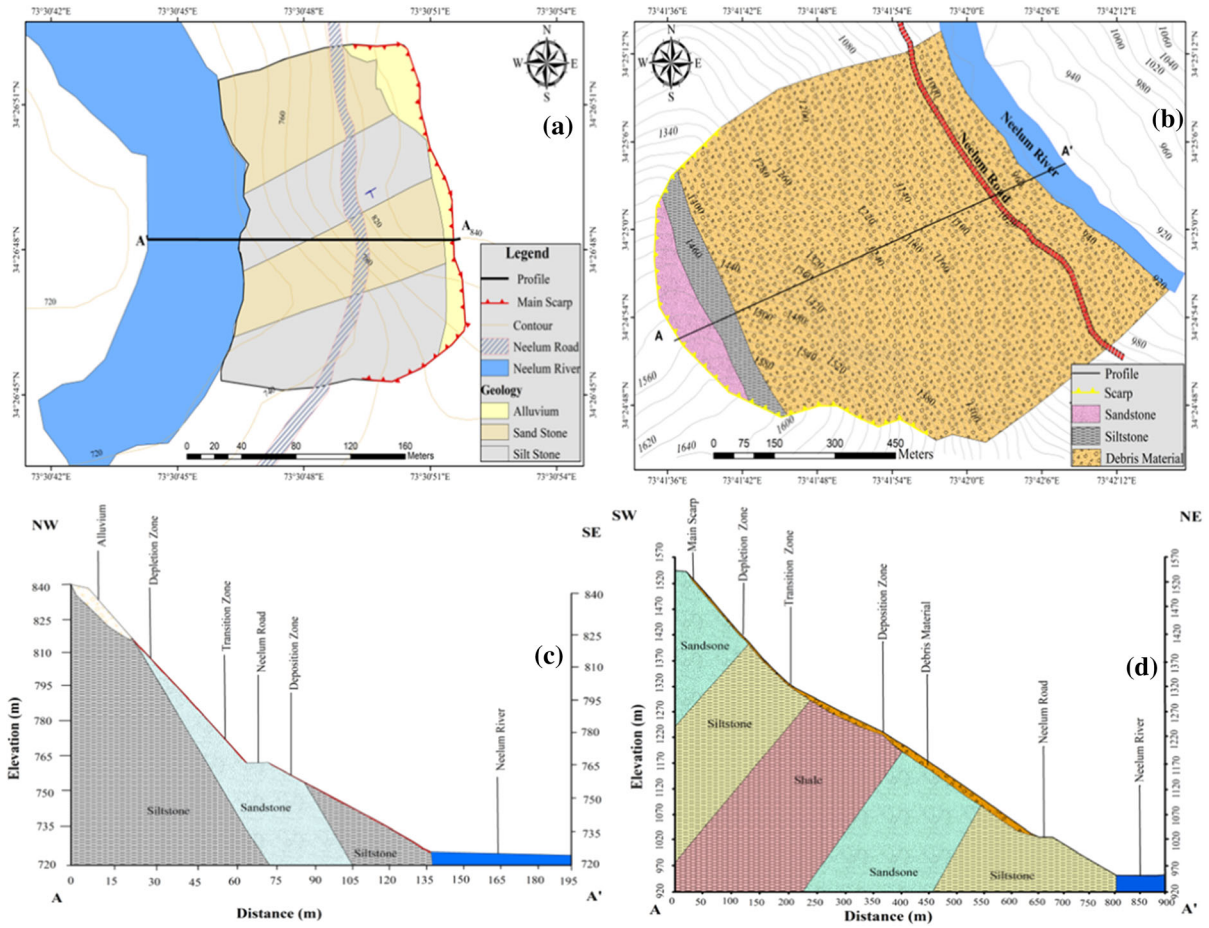

Fig. 5 **a** Geological map of Ghori landslide **b** Geological map of Dhanni landslide **c** longitudinal profile of Ghori landslide **d** longitudinal profile of Dhanni landslide

Longitudinal and cross profiles have been prepared by using the field data taken by laser distance meter shown in Fig. 5c,d. The profiles show the initiation of movement and the debris material exposed along the longitudinal and cross sections of the landslide. These longitudinal and cross profile have been used to understand the intact mass and the transported material along the landslide surface. The volume of landslides was roughly estimated by multiplying the landslide area with the average thickness. The thickness of the deposit was observed during field investigation and calculated from the construction of longitudinal and cross profiles. The total surface area and deposit area of landslides have been calculated using ArcGIS software after mapping.

Ghori landslide is located approximately 15 km in the north of the capital city of the Muzaffarabad along the main Neelum Valley road, AJK. It is bounded by longitude 73° 30′ 42″ to 73° 30′ 54″ N and latitudes 34° 26′ 44″ to 34° 26′ 52″ E (Fig. 4a). The landslide occurs in the Miocene Murree Formation. The Murree Formation consists of interbedded sandstone, siltstone, shale, and clays. The lithostratigraphic units exposed at the locality of the landslide are sandstone, siltstone, and shales of Murree Formation. The strike of the sandstone bed is trending from NE to SW and dipping in SE direction. Dip angle ranges from 40 to 50°. The main body of the landslide contains mainly shale fragments with abundant gravel, pebble and cobble fractions of sandstone.

The material of landslide moved from the source area and traveled towards the valley floor. However, the debris material remained deposited in the middle and lower part of the main slide. In the middle portion

of the slide just along the road and below the road, the sandstone and siltstone exposures are present within the debris material. The bedrock of sandstone is exposed on the road cut and also below the road. The thickness of debris material is about 3–4 m. The total surface area of the landslide is calculated about 26,082 m^2 (Table 1).The elevation measured from top to toe is 120 m. The landslide was initiated at the elevation about 840 m above sea level (asl) and traveled towards the Neelum River.

Dhanni landslide is located approximately 10 km in the south of district Neelum, along the main Neelum Valley road, AJK. It is bounded by longitude 73° 41′ 35″ to 73° 42′ 15″ N and latitudes 34° 24′ 45″ to 34° 25′ 10″ E (Fig. 4b). The landslide also occurs in the Miocene Murree Formation. The strike of the sandstone bed is trending from NE to SW and dipping in SE direction. Dip angle ranges from 35 to 40°. There was multiple drainage channels developed in the main body of the landslide. The Neelum Road is located at about 180 m from the river. The length of the landslide is about 850 m. In the middle portion of the slide just along the road and below the road, the sandstone and siltstone exposures are present within the debris material. The bedrock of sandstone is exposed on the road cut and also below the road. The thickness of debris material is about 8–10 m. The total surface area of the landslide is calculated about 567,735 m^2 (Table 1).The elevation measured from top to toe is 630 m. The landslide was initiated at the elevation about 1550 m asl and traveled towards the Neelum River. Tension cracks (Fig. 2d) with 1–2 m in length were found on the scarp and the main body of the landslides which might be the initiation for the future landslides.

Table 1 Geometric characteristics of the landslides

	Ghori landslide	Dhanni landslide
Crown elevation (m)	840	1550
Length(m)	138	850
Width (m)	190	650
Estimated depth (m)	3–4	8–10
Height (m)	120	630
Total surface area (m^2)	26,082	56,7735
Deposit area (m^2)	8561	25,3504
Estimated volume (m^3)	10,4328	56,77,350
Geological period	Miocene	Miocene

4 Materials and Methods

4.1 Soil Samples

Two samples were collected from the main body of the landslides above the Neelum valley road (Fig. 4a, b), about 10 kg each and were packed in airtight plastic bags. The samples were transported to Japan for laboratory testing.

Grain size distribution of the soil samples derived from the landslide sites are shown in Fig. 6. For the triaxial tests, we used a cylindrical specimen of 50 mm in diameter and 100 mm in height. In order to achieve the sufficient reproducibility of the tests, we sieved the sample so that the maximum particle size becomes less than 1/20 of the size of the specimen. For this, the particle size distribution is set to pass through sieve no. 10 (the particle diameter of 2.00 mm). Dhanni landslide specimen after sieving has specific gravity of soil particles, G_s, of 2.71, maximum specific volume, v_{max}, of 1.79, minimum specific volume, v_{min}, of 1.45, mean grain size, D_{50}, of 0.74 mm, uniformity coefficient, U_c, of 6.50. Dhanni soil specimen has 5.0% fine fraction consisting of non-plastic particles. Ghori landslide specimen has specific gravity, G_s, of 2.65, maximum specific volume, v_{max}, of 1.72, minimum specific volume, v_{min},of 1.33, mean grain size, D_{50}, of 0.7 mm, uniformity coefficient, U_c, of 4.0. Ghori soil specimen has 3.0% fine fraction and is a non-plastic material. The physical properties and grain size accumulation curve are summarized in Table 2 and Fig. 6, respectively.

All the tests were conducted on re-compacted specimens with the initial relative density of 90% for both specimens from two landslide sites (the initial dry density of 1.93 g/cm^3 for the sample from Ghori landslide and 1.89 g/cm^3 for the sample from Dhanni landslide).

4.2 Testing Apparatus

The test apparatus used in this study consists of a double-walled triaxial cell, an axial loading device, pore-air, and cell pressure and volume change measuring devices, and a computer program for

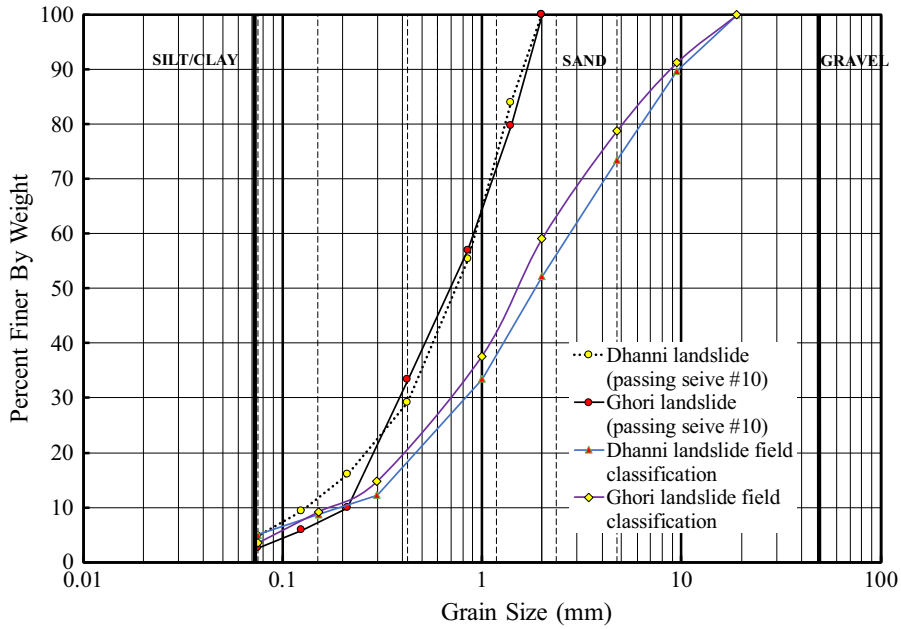

Fig. 6 Grain size distribution of soils collected from the middle of Ghori and Dhanni landslide

Table 2 Physical properties of the tested material

	Dhanni landslide	Ghori landslide
Specific gravity, Gs	2.71	2.65
Maximum dry density, ρ_{dmax} (g/cm^3)	1.87	1.99
Minimum dry density, ρ_{dmin} (g/cm^3)	1.51	1.54
Minimum specific volume, v_{min}	1.45	1.33
Maximum specific volume, v_{max}	1.79	1.72
Liquid limit, w_l (%)	15.0	19.5
Plastic limit, w_p (%)	NP	NP

controlling test sequence and recording data, as shown in Fig. 7.

The axial displacement is measured externally by an LVDT (Linear Variable Displacement Transducer). The overall volume change of the sample is measured by the double-cell technique. The double cylinder system in the triaxial apparatus consists of an inner cell (Fig. 7) coaxial to the sample and filled with water. The variations in the level of water in the inner cell can be used to obtain the volume change of the sample. The system can apply deviatoric stress in strain-controlled condition, and it is measured by the load cell with the capacity of 5 kN located above the top cap (Figs. 7, 8a). In the wetting stage of the soil sample, carbon dioxide (CO_2) was first passed from the bottom to the top of the sample. The sample was then saturated by sending de-aired water under a small hydraulic head difference.

4.3 Measurement and Arrangement of the Results

Axial strain, ϵ_a, volumetric strain, ϵ_v, axial stress, σ'_a, and radial stress,σ'_r,are measured during the experiment. Considering the axisymmetric stress condition in the triaxial tests, other variables are calculated using the measured variables as follows.

Mean effective stress is given as:

$$p' = \frac{\mathrm{tr}\boldsymbol{\sigma}'}{3} = \frac{\sigma'_a + 2\sigma'_r}{3}$$

where σ' is the effective stress tensor. Deviator stress q is given as:

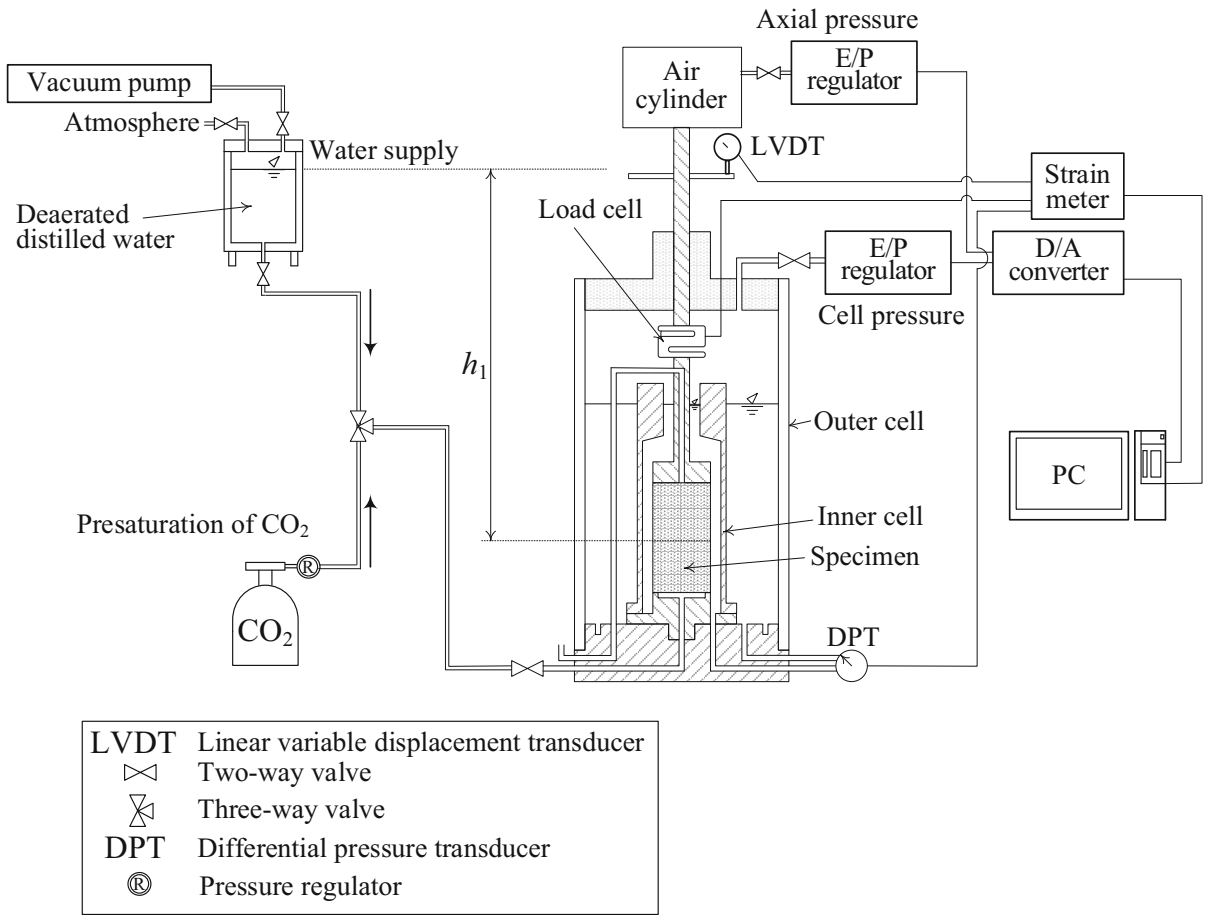

Fig. 7 Schematic figure of the triaxial testing apparatus with wetting path and double-cell type volume measurement system

$$q = \sqrt{\frac{3}{2}\mathbf{s} : \mathbf{s}} = \sqrt{\frac{3}{2}(\boldsymbol{\sigma}' - p'1) : (\boldsymbol{\sigma}' - p'1)}$$

where $\mathbf{s}\left(= \boldsymbol{\sigma}' - p'1\right)$ is deviator stress tensor and 1 is a unit second order tensor. Stress ratio is given as follows.

$$\eta = \frac{q}{p'}$$

Meanwhile, volumetric strain is defined as:

$$\epsilon_v = \mathrm{tr}\boldsymbol{\epsilon} = \epsilon_a + 2\epsilon_r$$

where ϵ_r is radial strain. Thus, radial strain, ϵ_r is obtained by:

$$\epsilon_r = \frac{\epsilon_v - \epsilon_a}{2}$$

The deviator strain, ϵ_d,is calculated as follows.

$$\epsilon_d = \sqrt{\frac{2}{3}\mathbf{e} : \mathbf{e}} = \sqrt{\frac{2}{3}\left(\boldsymbol{\epsilon} - \frac{\epsilon_v}{3}1\right) : \left(\boldsymbol{\epsilon} - \frac{\epsilon_v}{3}1\right)}$$

where $\boldsymbol{e}\left(= \boldsymbol{\epsilon} - \frac{\epsilon_v}{3}1\right)$ is deviator strain tensor.

4.4 Testing Procedure

First, fixing the pedestal to the base plate of the triaxial cell, a 0.3 mm thick rubber membrane was set to the circumference of the pedestal by O-rings. The membrane was then stretched with the help of the split mold by giving a suction pressure of 10 kPa, and the specimen was prepared on the top of the porous stone by the method of dry tamping in six equal layers. Then set the position of loading ram to the loading head precisely and tightens the rubber membrane with the loading piston and increased the suction pressure to 25 kPa. At this stage, sample preparation was completed.

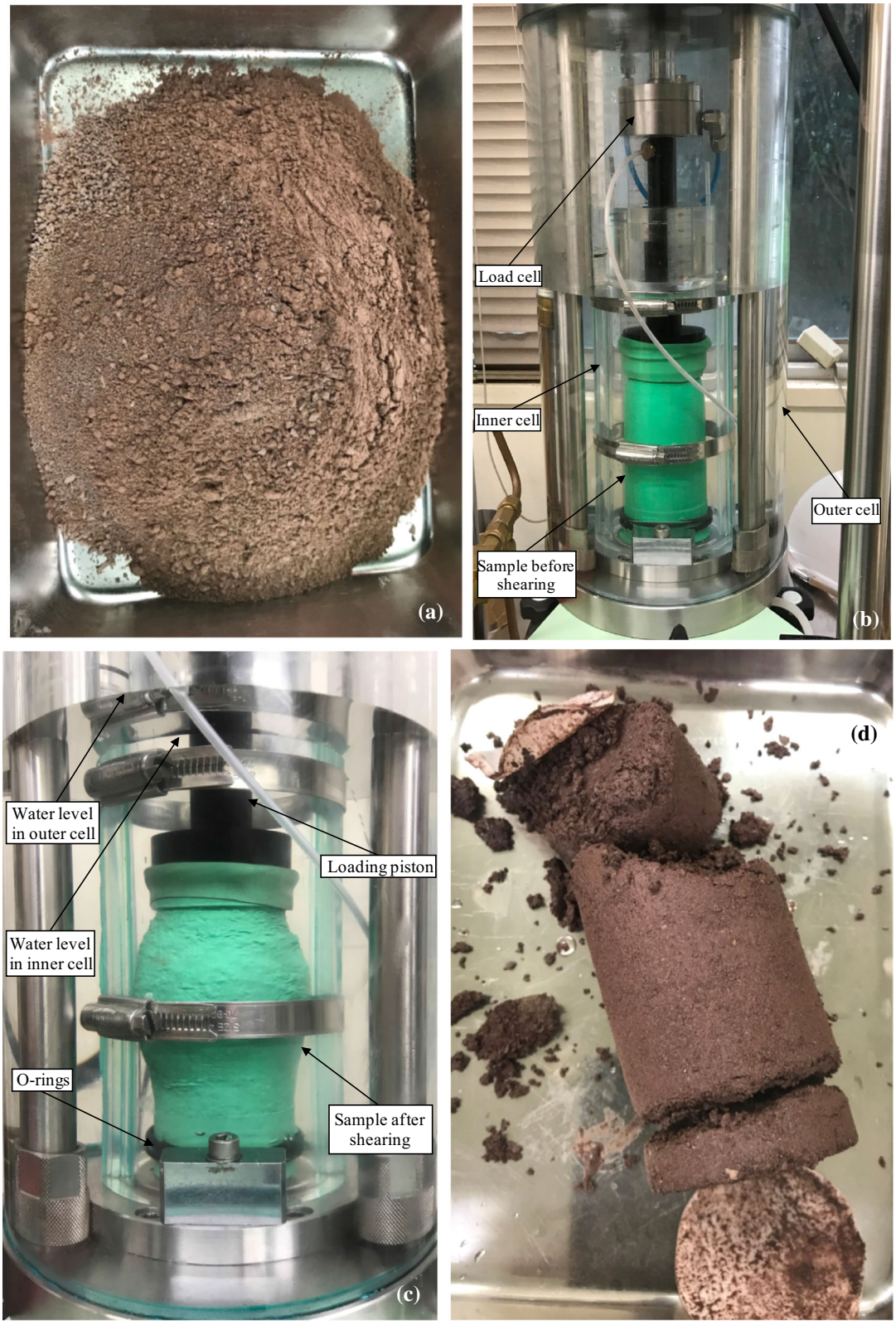
(a)
Load cell
Inner cell
Outer cell
Sample before shearing
(b)
Water level in outer cell
Loading piston
Water level in inner cell
O-rings
Sample after shearing
(c)
(d)

◀**Fig. 8** **a** Soil sample before testing, **b** soil specimen after consolidation, **c** bulging failure of soil specimen after shearing, and **d** soil specimen after testing

Isotropic consolidation had been performed as an initial stage of the consolidated drained triaxial tests, and stepwise increase in mean effective stress had been applied from 25 to 400 kPa. The peak deviator stress,q_{max}, of the material derived from each landslide was obtained by the drained, monotonic shearing test on a dry specimen. The monotonic shearing has performed up to 25% of the total axial strain is achieved. As all other tests were conducted on the sample with the same initial density, the stress–strain behavior before soaking (isotropic compression and shearing under dried condition) of the tests for each material looked to be almost identical and sufficiently high reproducibility could be achieved. In total, six tests were performed on Ghori slide sample and five tests on Dhanni slide sample, for which we varied deviatoric stress, q, during water infiltration stage. The inner cell shown in Fig. 8 was filled with distilled, de-aired water and the outer cell was filled with distilled water. The test is focused on the volumetric compression during compression, shearing and water infiltration stages during the triaxial test. The volumetric strain is detected by measuring the change of the water level inside the inner cell during the experiment. Furthermore, with a constant loading rate of 0.5 cm/min, the shear process performed under mean effective stress constant (p' constant).

In the Himalayan region, slopes remain in a relatively dried state most of the time during the year, but landslides usually occur in shallow vadose zones due to heavy rainfall during monsoon season (June–August) as shown in Fig. 3b. To simulate such process, the dry samples were saturated under different stress conditions without any particular change in pore pressure. CO_2 was first passed through the specimen slowly for 30 min to remove any air from the voids, after which de-aired water was permeated very slowly through the specimen for 24 h by applying a total water head difference, h_1, of around 20 cm. Water was infiltrated into the specimen at 0, 22, 33, 44, 77, and 88% of the maximum deviatoric stress of each specimen, which corresponds a stress ratio,η, of 0.0, 0.4, 0.6, 0.8, 1.4 and 1.6, respectively. Throughout the entire testing process, the samples were allowed to drain freely. The soil specimen weighed at the beginning and end of each test to calculate the final moisture content for each test.

5 Results and Discussions

Figures 9 and 10 show the results of CD triaxial tests on the soil samples from Ghori and Dhanni, respectively. As the same initial relative density is achieved for all the cases, all stress–strain curves traced an identical isotropic compression curve and exhibited a very similar shearing behavior before reaching a prescribed stress ratio as shown in Figs. 9b and 10b.

Figures 9b and 10b illustrated the relationship between deviatoric stress and axial strain for the unsaturated compacted soil specimen and the specimens with water infiltration for Ghori and Dhanni landslides. The maximum deviatoric stress for each sample was obtained from the monotonic shearing test on dried sample, respectively. The stress–strain relationships due to shearing and water infiltration under mean principal stress constant (p) are shown in figures and the relationships of all the specimens are almost identical and this reveals high reproducibility of the tests. The specimen exhibited hardening behavior with negative dilation in the beginning and showed very slight softening with slight dilation.

The Figs. 9b and 10b are showing the characteristics of monotonic shear and water infiltration under mean principal stress (p') constant. The axial strain (ε_a) of Ghori landslide specimen during monotonic shear is reached to 2.46, 2.68, 3.69, 5.54, and 7.16% subjected to q = 160, 240, 320, 560, and 640 kPa, respectively, while the axial strain of Dhanni landslide specimen is reached of 3.43, 3.89, 4.75 and 7.75% respectively before water infiltration. The axial strain was increased simultaneously during isotropic compression and shearing stage, but it increased rapidly immediately after water infiltration and then gradually slows down and take about 20–22 h (average for each test) to become stationary after wetting. It is also observed that the axial strain of Ghori landslide specimen is lower than Dhanni landslide specimen in each case subject to the same deviatoric stress (q).The sample preparation and testing conditions are the same for both the specimens except the initial dry density. Dhanni landslide has less dry density as compared to Ghori landslide. It can be said that for the same

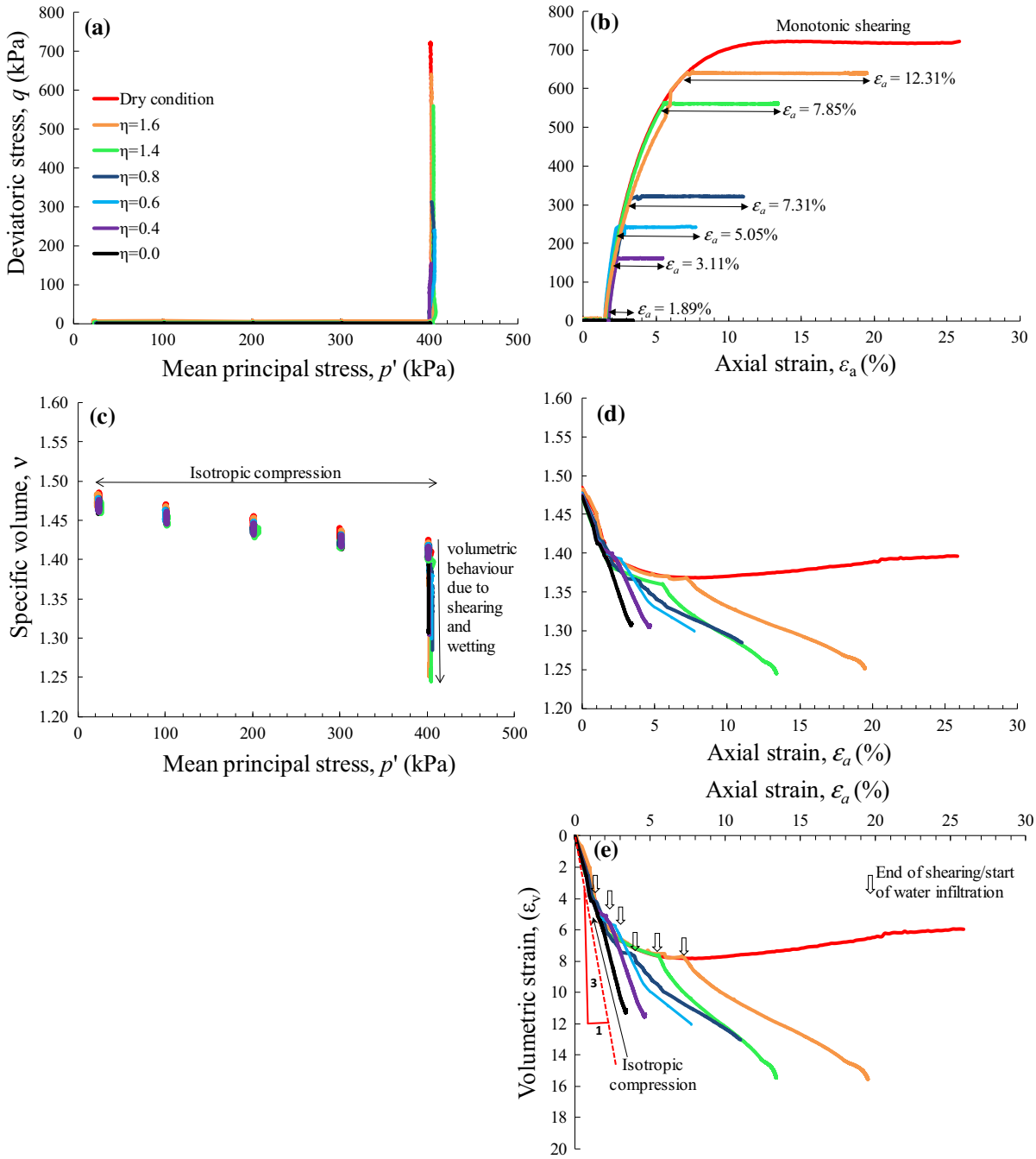

Fig. 9 CD triaxial test results of Ghori landslide

deviatoric stress state under which wetting process occurs, lower values of density leads to the more substantial strain or failure of soil.

For all the cases, by keeping the deviatoric stress constant at different stress levels (stress ratio of 0.0, 0.4, 0.6, 0.8, 1.4, 1.6), axial strain was increased due to water infiltration by an amount of 1.89, 3.11, 5.05, 7.31, 7.85, 12.31% respectively for Ghori landslide and 2.63, 3.89, 6.08, 7.34, 14.61% respectively for Dhanni landslide. Therefore, it is revealed that the

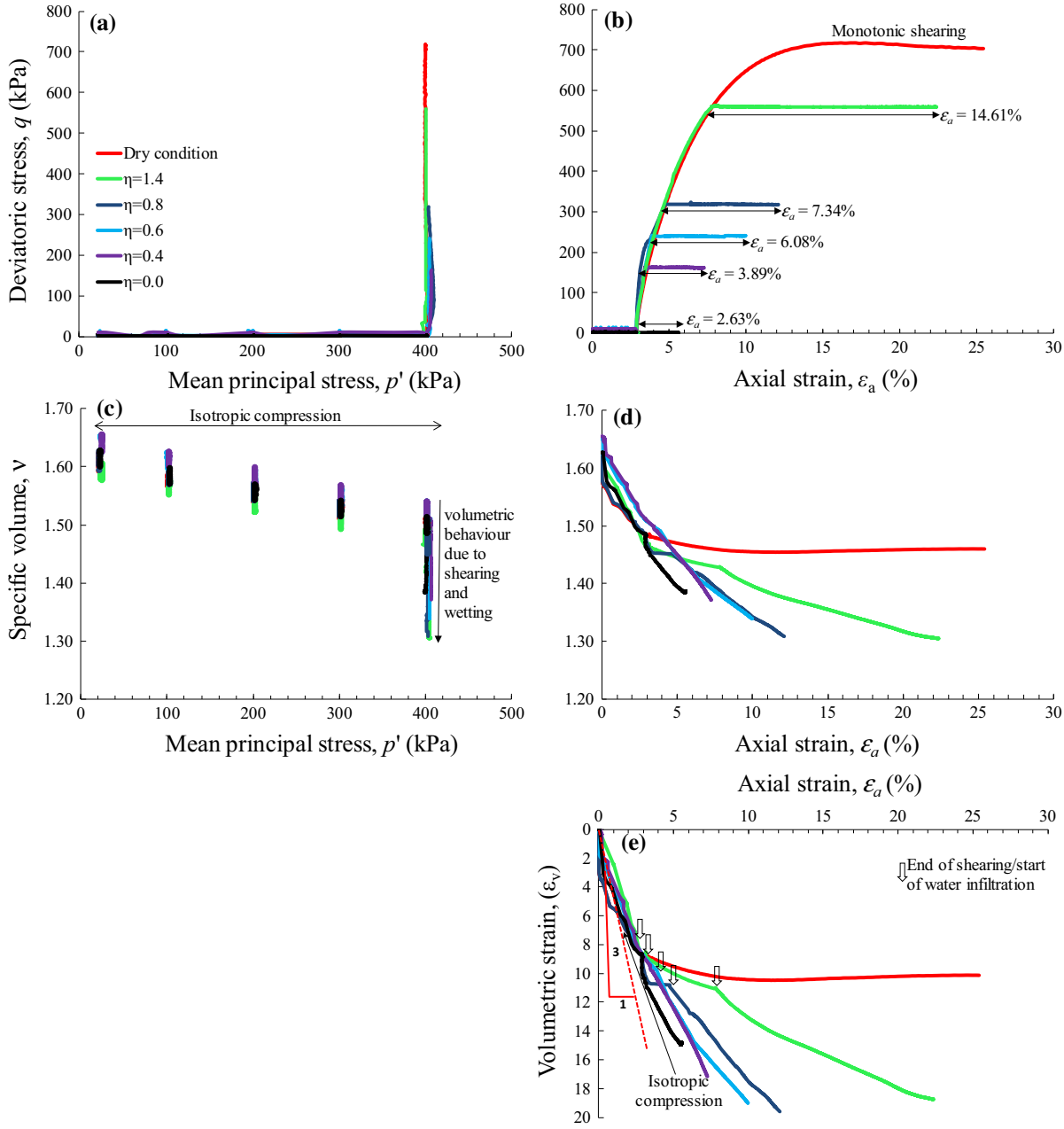

Fig. 10 CD triaxial test results of Dhanni landslide

wetting axial strain increases for both the samples with the increase in deviator stress ratio at wetting for the same confining stress. In the case of stress ratio of $\eta = 0.0$, water infiltration was carried right after isotropic consolidation at constant zero deviatoric stress. Therefore, a decidedly less axial strain was produced shown by the black color line in Figs. 9b and 10b. The increase in the axial strain without further application of shear stress results in deformation of soil. Therefore, it can be said that deformation of soil should be considered while analyzing the soil behavior due to water infiltration.

In Figs. 9 and 10, section (c) and (d) showed the relationship of specific volume with mean effective

stress and axial strain for the samples from Ghori and Dhanni landslides, respectively. Isotropic compression was first applied, and triaxial compression test was performed under drained-air condition viz keeping mean effective stress constant after the deviator stress reached a prescribed value. The figures show that both specimens had undergone various degree of softening due to wetting at different stress levels under p and q keeps constant. Furthermore, during isotropic compression, monotonic shear and water infiltration phase, the increase of axial strain leads to the decrease of the specific volume. The initial specific volumes of the specimens varied around 0.03–0.04 (Dhanni specimens varied up to around 0.05) and the compression lines are almost linear and parallel to each other. This clearly shows that the samples had almost same initial density and the reproducibility of the tests is quite sufficient.

In Figs. 9 and 10, section (e) illustrated the changes of the volumetric strain with axial strain for the isotropic compression, shearing, and water infiltration stage of Ghori and Dhanni landslides. Axial and lateral deformations have been produced during the wetting phase; however, contracting volumetric deformation is considerable due to the lateral expansion of the specimen as shown in Fig. 8b.These results indicate that the soil specimen before water infiltration displays the behavior as that the soil behavior in non-infiltration tests. After water infiltration, the soil goes into a plastic state. The change in volume of the specimen in case of infiltration test under constant deviatoric stress depends on deviatoric stress level; the volume increases with increase in stress ratio, η, i.e., 0.0, 0.4, 0.6, 0.8, 1.4, and 1.6 for each specimen. It was also observed that volume increases with an increase in axial strain level and specimen did not follow the same path after infiltration. The volume increase continues, and all specimens followed the parallel paths after water infiltration as shown in Fig. 9e and 10e for Ghori and Dhanni landslides respectively. It has pointed out that the behavior of both the specimen during initial compression was isotropic as the ratio of both strains was satisfied ($\varepsilon_v = 3\varepsilon_a$), while anisotropic behavior occurred during water infiltration since the softening behavior appeared during wetting. Infiltration of water into the sample was applied vis keeping deviator stress constant. All the samples showed volumetric compression as shown in Figs. 9e and 10e. In Figures, the slope of 3 means the isotropic compression of the sample (as axial strain increment is equal to radial strain increment): the soil sample exhibited isotropic compression under isotropic stress condition; the axial strain slope becomes smaller under higher deviator stress level and the soil exhibits distortional behavior under anisotropic compression. The wetting-induced deformation becomes anisotropic and the distortional strain generated due to wetting becomes more significant under higher deviator stress. So the soil exhibits compressive-distortional behavior under higher deviator stress, which corresponds to the failure behavior of the soil in steeper slope.

On the other hand, soil behavior during the wetting process at higher deviatoric stress state is a viscous Behavior. For example, the volumetric behavior of soil in Fig. 10e at $0.8q_{max}$ (shown by the blue line) and $1.4q_{max}$ (shown by the green line) indicates the collapse of soil faster at $1.4q_{max}$ than the $0.8q_{max}$. Considering volumetric behavior of specimens during water infiltration shown in Figs. 9 and 10, we can say that deformation of soil due to water infiltration is a critical phenomenon, even if the soil is not failed, significant deformations are observed due to water infiltration.

Figure 11a illustrates the variation of wetting axial ($d\varepsilon_a$) and wetting radial strains ($d\varepsilon_r$) with different stress ratios (η) for Ghori and Dhanni landslides. Wetting axial and radial strains are the variation in the strains during water infiltration. It is evident that by keeping the deviator stress constant, wetting-induced deformations of both soils is almost isotropic under isotropic stress condition, while incremental axial strain increases and radial strain decreases with the increase in the stress ratio. Both incremental axial and radial strains due to wetting become more significant under higher stress ratio for both the samples.

Figure 11b depicts the variation in wetting volumetric strain ($d\varepsilon_v$) with different stress ratios. It is clearly shown that wetting induced deformations of both soils were compressive. The volume change slightly increases with the increase in stress ratio at the beginning for both specimens but not much different.

The effect of stress ratio on the wetting induced distortional behavior of Ghori and Dhanni landslide specimens is shown in Fig. 11c. The figure shows that wetting caused significant distortional deformation under higher stress ratio, which implies significant shearing deformation is expected to occur under

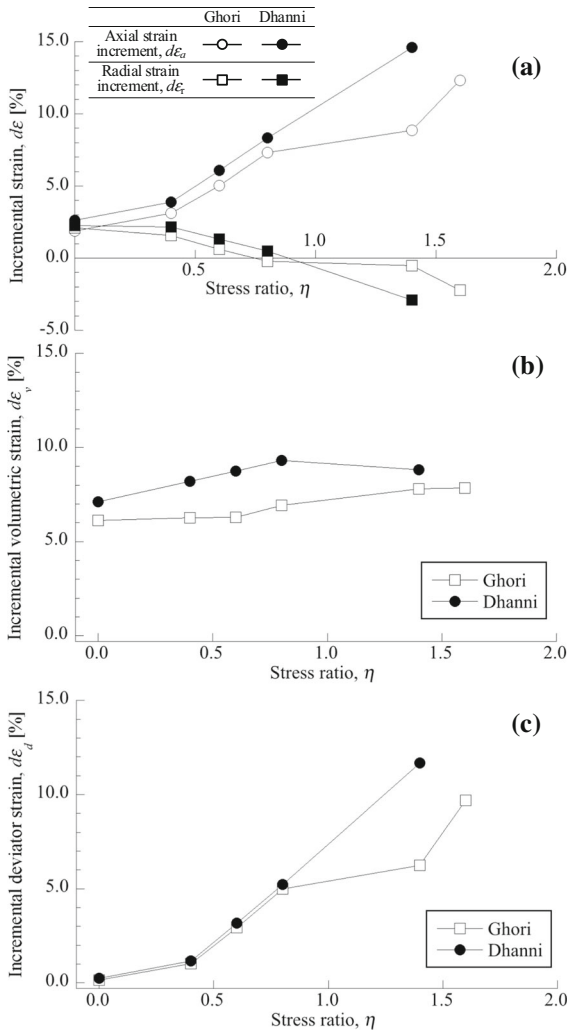

Fig. 11 Wetting-induced deformation of soils of Ghori and Dhanni landslide with deviatoric stress ratio

anisotropic stress state such as in ground near the steep slope.

6 Conclusions

The response of two kinds of the samples derived from two actual landslide sites in Kashmir, Pakistan, has been investigated through a series of laboratory element tests. The soil samples were initially dry condition, and the anisotropic stress states that are assumed in the stress condition in the slope were applied by shearing the samples under drained-air condition. The soils were then subjected to water infiltration under various levels of constant deviatoric stress to model the wetting of the ground due to rainfall. Some conclusion can be drawn from the study a as follows,

1. Wetting cause significant deformation regardless of the stress condition even effective stress remains constant.
2. Wetting-induced deformation under isotropic stress conditions significantly compressive, but the deformation was almost isotropic. Thus, soil exhibits significant compression but never fails under isotropic stress state.
3. Wetting-induced deformation under anisotropic stress condition is both compressive and distortional. Under higher deviator stress, magnitudes of incremental deviatoric strain becomes much larger while those of volumetric compression become slightly larger.
4. Practical meaning and significance of the results can be summarized as follows: Significant volumetric compression of soil due to water infiltration is a critical phenomenon regardless of the stress state. The experimental results reveal the mechanism of the slope failure. Even without significant change in effective stress, rainfall or rise in groundwater level will wet the ground; the wetting of the ground affects the mechanical behavior of soil, and this cause significant deformation and failure of slopes in the actual field. Especially in steeper slope, stress state tends to be anisotropic and stress ratio tends to be higher, which results in higher risk in slope failure.

Acknowledgements The first author would like to thank Pakistan metrological Department, Lahore office and planning and development department (PDD) Muzaffarabad, Azad Jammu and Kashmir for providing rainfall and landslide data. A debt of gratitude is also owed to Mr. Muhammad Shehzad Khalid for his assistance in field investigation and sampling from the landslide site. This work has been supported by JSPS KAKENHI Grant No. 16H06099 provided to the second author.

References

Albrecht BA, Benson CH (2001) Effect of desiccation on compacted natural clays. J Geotech Geoenviron Eng 127:67–75

Anderson SA, Riemer MF (1995) Collapse of saturated soil due to reduction in confinement. J Geotech Eng 121(2):216–220

Aydan Ö, Ohta Y, Hamada M (2009) Geotechnical evaluation of slope and ground failures during the 8 October 2005 Muzaffarabad earthquake, Pakistan. J Seismol 13:399–413

Basharat M, Rohn J, Baig MS, Khan MR (2014) Spatial distribution analysis of mass movements triggered by the 2005 Kashmir earthquake in the Northeast Himalayas of Pakistan. Geomorphology 206:203–214

Bishop AW, Donald IB (1961) The experimental study of partly saturated soil in the triaxial apparatus. In: Proceedings of the 5th international conference on soil mechanics and foundation engineering, Paris, vol 1, pp 13–21

Bulmer M, Farquhar T, Roshan M, Akhtar SS, Wahla SK (2007) Landslide hazard after the 2005 Kashmir earthquake. EOS Trans 88:53–55

DeCarlo KF, Shokri N (2014) Effects of substrate on cracking patterns and dynamics in desiccating clay layers. Water Resour Res 50(4):2039–3051

During the event of rainfall (2005) Muzaffarabad earthquake, Pakistan. J Seismolol 13:399–413

Elsharief AM, Mohamedzein EA, Saad SH (2016) Effects of wetting on the shear strength of plastic silty sands. In: Proc. of the 4th geo-China international conference, pp 148–156

Farulla A, Ferrari C, Romero AE (2010) Volume change behaviour of a compacted silty clay during cyclic suction changes. Can Geotech J 47(6):688–703

Ferber V, Auriol JC, Cui YJ, Magnan JP (2008) Wetting induced volume changes in compacted silty clays and high plasticity clays. Can Geotech J 45(2):265–252

Fujiwara S, Tobita M, Sato HP, Ozawa S, Une H, Koarai M, Nakai H, Fujiwara M, Yarai H, Nishimura T, Hayashi F (2006) Satellite data gives snapshot of the 2005 Pakistan earthquake. EOS Trans Am Geophys Union 87:73–77

Guzzetti F, Carrara A, Cardinali M, Reichenbach P (1999) Landslide hazard evaluation: a review of current techniques and their application in a multi-scale study, Central Italy. Geomorphology 31:181–216

Jennings JEB, Burland JB (1962) Limitations to the use of effective stresses in partly saturated soils. Geotechnique 12(2):125–144

Kamp U, Growley BJ, Khattak GA, Owen LA (2008) GIS-based landslide susceptibility mapping for the 2005 Kashmir earthquake region. Geomorphology 101:631–642

Kamp U, Owen L, Growley B, Khattak G (2010) Back analysis of landslide susceptibility zonation mapping for the 2005 Kashmir earthquake: an assessment of the reliability of susceptibility zoning maps. Nat Hazards 54:1–25

Kato, A., Ohnaka, M., 2000. Effect of water on stability or instability of the shear fracture process of rock. Journal of Geography 109(4), 554–563

Konagai K, Sattar A (2011) Partial breaching of Hattian Bala landslide dam formed in the 8th October 2005 Kashmir earthquake, Pakistan. Landslides 9:1–11

Konagai K, Jorgen J, Shigeki T, Takaaki I (2009) Huge landslides caused by massive earthquakes and long-lasting geotechnical risks. In: Sassa K, Canuti P (eds) Landslides – disaster risk reduction. Springer, Berlin, Heidelberg, pp. 159–176

Leonards GA, Davidson LW (1984) Reconsideration of failure initiating mechanisms for Teton Dam. In: Proceedings of the international conference on case histories in geotechnical engineering, Missouri, USA, vol 2, pp 1103–1113.

Leonards GA, Narain J (1963) Flexibility of clay and cracking of earth dams. ASCE 89(2):47–98

Lim YY, Miller GA (2004) Wetting-induced compression of compacted Oklahoma soils. J Geotech Geoenviron Eng 130:1014–1023

Meen WG, Young MW (2014) Failure of soil underwater infiltration condition. Eng Geol 181:124–141

Meilani I, Rahardjo H, Leong EC (2005) Pore-water pressure and water volume change of an unsaturated soil under infiltration conditions. Can Geotech J 42(6):1509–1531

Melinda F, Rahardjo H, Han KK, Leong EC (2004) Shear strength of compacted soil under infiltration condition. J Geotech Geoenviron Eng 130(8):807–817

Miller GA, Muraleetharan KK, Lim YY (2001) Wetting induced settlement of compacted fill embankments. Transp Res Rec 1755:111–118

Nishigata T, Nishida K, Araki S (2003) Behavior of unsaturated decomposed granite soil during water infiltration. In: Proceedings of the 3rd international conference on unsaturated soils, pp 563–568

Osanai N, Tomita Y, Akiyama K, Matsushita T (2009) Reality of cliff failure disaster. Technical Note of National Institute for Land and Infrastructure Management, p 530

Owen LA, Kamp U, Khattak GA, Harp EL, Keefer DK, Bauer MA (2008) Landslides triggered by the 8 October 2005 Kashmir earthquake. Geomorphology 94:1–9

Peduzzi P (2010) Landslides and vegetation cover in the 2005 North Pakistan earthquake: a GIS and statistical quantitative approach. Nat Hazard 10:623–640

Pereira JHF, Fredlund DG (2000) Volume change behavior of collapsible compacted gneiss soil. ASCE 126(10):907–916

Petley D, Dunning S, Rosser N, Kausar AB (2006a) Incipient landslides in the Jhelum Valley, Pakistan following the 8th October 2005 earthquake. In: Marui H (ed) Disaster mitigation of debris flows, slope failures and landslides, Frontiers of science series. Universal Academy, Tokyo, Japan.

Petley D, Dunning S, Rosser N, Kausar AB (2006b) Incipient landslides in the Jhelum Valley, Pakistan following the 8th October 2005 earthquake. In: Disaster mitigation of rock flows, slope failures and landslides. Universal Academy Press, pp 1–9

Prakoso WA (2013) Wetting effect on CBR properties of compacted fine-grained residual soils. In: Foundation engineering in the face of uncertainty, Geo-Congress, San Diego, pp 354–367.

Rahman A-U, Khan A, Collins A (2014) Analysis of landslide causes and associated damages in the Kashmir Himalayas of Pakistan. Nat Hazards 71:803–821

Ray PKC, Parvaiz I, Jayangondaperumal R, Thakur VC, Dadhwal VK, Bhat FA (2009) Analysis of seismicity-induced landslides due to the 8 October 2005 earthquake in Kashmir Himalaya. Curr Sci 97:1742–1751

Riaz S, Wang G, Basharat M, Takara K (2019) Experimental investigation of a catastrophic landslide in northern Pakistan. Landslides 16:2017–2032

Saba SB, van der Meijde M, van der Werff H (2010) Spatiotemporal landslide detection for the 2005 Kashmir earthquake region. Geomorphology 124:17–25

Sato HP, Hasegawa H, Fujiwara S, Tobita M, Koarai M, Une H, Iwahashi J (2007) Interpretation of landslide distribution triggered by the 2005 Northern Pakistan earthquake using SPOT 5 imagery. Landslides 4:113–122

Schneider J (2009) Seismically reactivated Hattian slide in Kashmir, Northern Pakistan. J Seismol 13:387–398

Shafique M, Meijde MV, Khan MA (2016) A review of the 2005 Kashmir earthquake induced landslides; from a remote sensing prospective. J Asian Earth Sci 118:68–80

Sudmeier-Rieux K, Jaboyedoff M, Breguet A, Dubois J (2011) The 2005 Pakistan earthquake revisited: methods for integrated landslide assessment. J Mountain Res Dev 31(2):112–121

Sun DA, Sheng D, Xu Y (2007) Collapse behaviour of unsaturated compacted soil with different initial densities. Can Geotech J 44(6):673–686

Tang CS, Wang DY, Shi B, Li J (2016) Effect of wetting-drying cycles on profile mechanical behavior of soils with different initial conditions. CATENA 139:105–116

USGS (United States Geological Survey). Magnitude 7.6 - Pakistan earthquake 2006 Summary. www.earthquake.usgs.gov

Wang G, Sassa K (2001) Factors affecting rainfall-induced landslides in laboratory flume tests. Géotechnique 51:587–600

Zhang H, Chen JK, Hu SW, Xiao YZ, Zeng BJ (2016) Deformation characteristics and control techniques at the shiziping earth core Rockfill dam. J Geotech Geoenviron Eng 142(2):1943–5606

Zhang K, Wu X, Niu R, Yang K, Zhao L (2017) The assessment of landslide susceptibility mapping using random forest and decision tree methods in the Three Gorges Reservoir area, China. J Environ Earth Sci. https://doi.org/10.1007/s12665-017-6731-5

Publisher's Note Springer Nature remains neutral with regard to jurisdictional claims in published maps and institutional affiliations.